Research Article | Vol. 7, No. 3 | 1 Mar 2017 | OPTICAL MATERIALS EXPRESS 785

Optical Materials EXPRESS

Hybrid nanodiamond and titanium dioxide nanobeam cavity design

KELVIN CHUNG,[1,*] TIMOTHY J. KARLE,[2] CHENG WANG,[3] MARKO LONČAR,[3] AND SNJEZANA TOMLJENOVIC-HANIC[1]

[1]School of Physics, The University of Melbourne, VIC 3010, Australia
[2]The Florey Institute of Neuroscience and Mental Health, VIC 3052, Australia
[3]John A. Paulson School of Engineering and Applied Sciences, Harvard University, MA 02138, USA
[*]kelvinc@student.unimelb.edu.au

Abstract: Titanium dioxide is an emerging optical material, with a relatively high refractive index ($n \sim 2$), which allows for high confinement of the electromagnetic field. Extensive research has been conducted on the negatively charged nitrogen vacancy centre in diamond due to its robust electronic and optical properties. In particular, its stable room-temperature photoluminescence properties have been considered for quantum optical applications. Nanobeam cavities are a geometry that offer exceptionally large-Q values given their minimal footprint, a must for high density and compact optical architecture. This paper presents an ultrahigh-Q nanobeam cavity within titanium dioxide in a low-refractive index environment operating at the negatively charged nitrogen vacancy centre of diamond. This research opens the possibility of hybrid optical devices utilising titanium dioxide and diamond.

OCIS codes: (230.1480) Bragg reflectors; (230.5298) Photonic crystals; (350.4238) Nanophotonics and photonic crystals.

References and links

1. G. Subramania, Y.-J. Lee, I. Brener, T. S. Luk, and P. G. Clem, "Nano-lithographically fabricated titanium dioxide based visible frequency three dimensional gap photonic crystal," Opt. Express **15**, 13049–13057 (2007).
2. G. Subramania, Y.-J. Lee, A. J. Fischer, and D. D. Koleske, "Log-pile TiO_2 photonic crystal for light control at near-UV and visible wavelengths," Adv. Mater. **22**, 487–491 (2010).
3. M. Furuhashi, M. Fujiwara, T. Ohshiro, M. Tsutsui, K. Matsubara, M. Taniguchi, S. Takeuchi, and T. Kawai, "Development of microfabricated TiO_2 channel waveguides," AIP Adv. **1**, 032102 (2011).
4. M. Furuhashi, M. Fujiwara, T. Ohshiro, K. Matsubara, M. Tsutsui, M. Taniguchi, S. Takeuchi, and T. Kawai, "Embedded TiO_2 waveguides for sensing nanofluorophores in a microfluidic channel," Appl. Phys. Lett. **101**, 153115 (2012).
5. Z.-F. Bi, L. Wang, X.-H. Liu, S.-M. Zhang, M.-M. Dong, Q.-Z. Zhao, X.-L. Wu, and K.-M. Wang, "Optical waveguides in TiO_2 formed by He ion implantation," Opt. Express **20**, 6712–6719 (2012).
6. J. D. B. Bradley, C. C. Evans, J. T. Choy, O. Reshef, P. B. Deotare, F. Parsy, K. C. Phillips, M. Lončar, and E. Mazur, "Submicrometer-wide amorphous and polycrystalline anatase TiO_2 waveguides for microphotonic devices," Opt. Express **20**, 23821–23831 (2012).
7. J. T. Choy, J. D. B. Bradley, P. B. Deotare, I. B. Burgess, C. C. Evans, E. Mazur, and M. Lončar, "Integrated TiO_2 resonators for visible photonics," Opt. Lett. **37**, 539–541 (2012).
8. F. Qiu, A. M. Spring, F. Yu, I. Aoki, A. Otomo, and S. Yokoyama, "Thin TiO_2 core and electro-optic polymer cladding waveguide modulators," Appl. Phys. Lett. **102**, 233504 (2013).
9. M. Häyrinen, M. Roussey, V. Gandhi, P. Stenberg, A. Säynätjoki, L. Karvonen, M. Kuittinen, and S. Honkanen, "Low-loss titanium dioxide strip waveguides fabricated by atomic layer deposition," J. Light. Technol. **32**, 208–212 (2014).
10. J. Park, S. K. Ozdemir, F. Monifi, T. Chadha, S. H. Huang, P. Biswas, and L. Yang, "Titanium Dioxide Whispering Gallery Microcavities," Adv. Opt. Mater. **2**, 711–717 (2014).
11. O. Reshef, K. Shtyrkova, M. G. Moebius, S. Griesse-Nascimento, S. Spector, C. C. Evans, E. Ippen, and E. Mazur, "Polycrystalline anatase titanium dioxide microring resonators with negative thermo-optic coefficient," J. Opt. Soc. Am. B **32**, 2288 (2015).
12. A. Paunoiu, R. S. Moirangthem, and A. Erbe, "Whispering gallery modes in intrinsic TiO_2 microspheres coupling to the defect-related photoluminescence after visible excitation," Phys. Status Solidi RRL **9**, 241–244 (2015).
13. C. C. Evans, C. Liu, and J. Suntivich, "Low-loss titanium dioxide waveguides and resonators using a dielectric lift-off fabrication process," Opt. Express **23**, 11160–11169 (2015).

#281097 https://doi.org/10.1364/OME.7.000785
Journal © 2017 Received 17 Nov 2016; revised 15 Dec 2016; accepted 26 Dec 2016; published 7 Feb 2017

Optical Materials EXPRESS

14. O. Carp, C. L. Huisman, and A. Reller, "Photoinduced reactivity of titanium dioxide," Prog. Solid State Chem. **32**, 33–177 (2004).
15. Z. Wang, U. Helmersson, and P.-O. Käll, "Optical properties of anatase TiO_2 thin films prepared by aqueous sol–gel process at low temperature," Thin Solid Films **405**, 50–54 (2002).
16. J. M. Bennett, E. Pelletier, G. Albrand, J. P. Borgogno, B. Lazarides, C. K. Carniglia, R. A. Schmell, T. H. Allen, T. Tuttle-Hart, K. H. Guenther, and A. Saxer, "Comparison of the properties of titanium dioxide films prepared by various techniques," Appl. Opt. **28**, 3303–3317 (1989).
17. A. D. Greentree, B. A. Fairchild, F. M. Hossain, and S. Prawer, "Diamond integrated quantum photonics," Mater. Today **11**, 22–31 (2008).
18. C. F. Wang, R. Hanson, D. D. Awschalom, E. L. Hu, T. Feygelson, J. Yang, and J. E. Butler, "Fabrication and characterization of two-dimensional photonic crystal microcavities in nanocrystalline diamond," Appl. Phys. Lett. **91**, 201112 (2007).
19. S. Schietinger, T. Schröder, and O. Benson, "One-by-one coupling of single defect centers in nanodiamonds to high-Q modes of an optical microresonator," Nano Lett. **8**, 3911–3915 (2008).
20. P. E. Barclay, K.-M. C. Fu, C. Santori, and R. G. Beausoleil, "Chip-based microcavities coupled to nitrogen-vacancy centers in single crystal diamond," Appl. Phys. Lett. **95**, 191115 (2009).
21. J. Wolters, A. W. Schell, G. Kewes, N. Nüsse, M. Schoengen, H. Döscher, T. Hannappel, B. Löchel, M. Barth, and O. Benson, "Enhancement of the zero phonon line emission from a single nitrogen vacancy center in a nanodiamond via coupling to a photonic crystal cavity," Appl. Phys. Lett. **97**, 141108 (2010).
22. A. Faraon, P. E. Barclay, C. Santori, K.-M. C. Fu, and R. G. Beausoleil, "Resonant enhancement of the zero-phonon emission from a colour centre in a diamond cavity," Nat. Photonics **5**, 301–305 (2011).
23. A. Faraon, C. Santori, Z. Huang, V. M. Acosta, and R. G. Beausoleil, "Coupling of nitrogen-vacancy centers to photonic crystal cavities in monocrystalline diamond," Phys. Rev. Lett. **109**, 033604 (2012).
24. B. J. M. Hausmann, B. J. Shields, Q. Quan, Y. Chu, N. P. De Leon, R. Evans, M. J. Burek, A. S. Zibrov, M. Markham, D. J. Twitchen, H. Park, M. D. Lukin, and M. Lončar, "Coupling of NV centers to photonic crystal nanobeams in diamond," Nano Lett. **13**, 5791–5796 (2013).
25. T. L. Wee, Y. W. Mau, C. Y. Fang, H. L. Hsu, C. C. Han, and H. C. Chang, "Preparation and characterization of green fluorescent nanodiamonds for biological applications," Diam. Relat. Mater. **18**, 567–573 (2009).
26. Y. Zhang and M. Lončar, "Ultra-high quality factor optical resonators based on semiconductor nanowires," Opt. Express **16**, 17400–17409 (2008).
27. P. B. Deotare, M. W. McCutcheon, I. W. Frank, M. Khan, and M. Lončar, "High quality factor photonic crystal nanobeam cavities," Appl. Phys. Lett. **94**, 12–15 (2009).
28. T.-W. Lu and P.-T. Lee, "Photonic crystal nanofishbone nanocavity." Opt. Lett. **38**, 3129–3132 (2013).
29. C.-S. Deng, Y.-S. Gao, X.-Z. Wu, M.-J. Li, and J.-X. Zhong, "Ultrahigh-Q TE/TM dual-polarized photonic crystal holey fishbone-like nanobeam cavities," Europhys. Lett. **108**, 54006 (2014).
30. D. Yang, P. Zhang, H. Tian, Y. Ji, and Q. Quan, "Ultrahigh-Q and low-mode-volume parabolic radius-modulated single photonic crystal slot nanobeam cavity for high-sensitivity refractive index sensing," IEEE Photonics J. **7**, 4501408 (2015).
31. S. Reitzenstein, C. Hofmann, A. Gorbunov, M. Strauß, S. H. Kwon, C. Schneider, A. Löffler, S. Höfling, M. Kamp, and A. Forchel, "AIAs/GaAs micropillar cavities with quality factors exceeding 150.000," Appl. Phys. Lett. **90**, 251109 (2007).
32. A. R. Md Zain, N. P. Johnson, M. Sorel, and R. M. De La Rue, "Ultra high quality factor one dimensional photonic crystal/photonic wire micro-cavities in silicon-on-insulator (SOI)," Opt. Express **16**, 12084–9 (2008).
33. Q. Quan, P. B. Deotare, and M. Lončar, "Photonic crystal nanobeam cavity strongly coupled to the feeding waveguide," Appl. Phys. Lett. **96**, 203102 (2010).
34. Q. Quan and M. Lončar, "Deterministic design of wavelength scale, ultra-high Q photonic crystal nanobeam cavities," Opt. Express **19**, 18529–18542 (2011).
35. Y. Akahane, T. Asano, B.-S. Song, and S. Noda, "High-Q photonic nanocavity in a two-dimensional photonic crystal," Nature **425**, 944–947 (2003).
36. W. Lukosz and R. Kunz, "Fluorescence lifetime of magnetic and electric dipoles near a dielectric interface," Opt. Commun. **20**, 195–199 (1977).
37. H. Chew, "Radiation and lifetimes of atoms inside dielectric particles," Phys. Rev. A **38**, 3410–3416 (1988).
38. Q. Quan, I. B. Burgess, S. K. Y. Tang, D. L. Floyd, and M. Lončar, "High-Q, low index-contrast polymeric photonic crystal nanobeam cavities," Opt. Express **19**, 22191 (2011).
39. M. W. McCutcheon, and M. Lončar, "Design of a silicon nitride photonic crystal nano cavity with a Quality factor of one million for coupling to a diamond nanocrystal," Opt. Express **16**, 19136 (2008).
40. T. van der Sar, J. Hagemeier, W. Pfaff, E. Heeres, S. Thon, H. Kim, P. Petroff, O. Tjerk, D. Bouwmeester, and R. Hanson, "Effect of a nanoparticle on the optical properties of a photonic crystal cavity: theory and experiment," J. Opt. Soc. Am. B **32**(4), 698–703 (2012).

Optical Materials EXPRESS

1. Introduction

Titanium dioxide (TiO_2) has recently emerged as a promising optical material in which waveguide and resonator structures have been fabricated [1–13]. It is a wide bandgap semiconductor with a bandgap energy range of 3–3.3 eV which is dependent on the crystalline phase [14]. It has a has a relatively high refractive index for visible wavelengths (n = 2.3 at 550 nm [15]), allowing for strong light confinement, and is also optically transparent. Amorphous and polycrystalline TiO_2 thin films can be deposited using conventional methods, such as electron-beam evaporation and ion sputtering [16], allowing for on-chip integration with other materials.

Diamond has garnered interest as a future photonic material [17] and has a similar refractive index to TiO_2. Research has focussed on enhancing the emission of the zero-phonon line (ZPL) of the negatively charged nitrogen vacancy (NV^-) colour centre [18–24]. The ZPL emission has a narrow linewidth which constitutes 3–5% of the total NV^- photoluminescence and enhancement can be achieved by coupling this emission to a high-Q optical cavity through the Purcell effect. The magnitude of enhancement is quantified by the Purcell factor which is dependent on the ratio between quality factor and modal volume ($\sim Q/V$); the larger this ratio, the greater the enhancement of the spontaneous emission rate.

Diamond substrates for photonic applications can be classified as either: individual micro- and nano-crystalline diamond (ND); polycrystalline diamond films and single-crystal diamond. The last classification is the leading candidate for diamond photonics, however it requires an intensive processing effort to engineer devices into the single crystal morphology. Individual ND have also attracted interest and the intrinsic fluorescence for the NV colour centre has been used for bioimaging applications [25]. Given the similar refractive indices of TiO_2 and diamond, it is a natural progression to combine both materials for hybrid applications where the former has already been shown to be an emerging visible photonic material [1, 2, 7, 10–13].

An optical cavity geometry that offers high-Q with minimal footprint is known as the nanobeam cavity; it is a photonic crystal cavity with periodic refractive index change in one-dimension. High-Q designs have been theoretically proposed (on the order of 10^7) [26–30] and experimentally demonstrated (in the order of 10^5) [27, 31, 32]. Previous high-Q designs generally considered high refractive index contrast environments ensuring the light was concentrated in the cavity region.

In this article, we present an ultrahigh-Q TiO_2 nanobeam cavity design with a quality factor in the order of 10^7 operating at the ZPL of NV^- of diamond. 3D FDTD simulations show that an ultrahigh-Q cavity is possible in this low refractive index contrast environment using a relatively simple design recipe.

2. TiO_2 nanobeam geometry and model

The design for this optical cavity was based on previous work by Quan *et al.* [33,34] which has a design philosophy following three main rules: (1) the cavity length should be zero, i.e. no defect is introduced into the periodicity; (2) the periodicity was kept constant; and (3) the requirement for a modulated Bragg mirror (referred in the rest of this letter as the Gaussian mirror). Rule (1) ensures the modal volume (V) is kept to a minimum alongside a high-Q cavity will result in a large Q/V ratio necessary for strong cavity interactions. Rule (2) guarantees a constant phase velocity between the periodic elements, i.e. the airholes. Finally, rule (3) results in a gentle modulation of the electric field between the Bragg mirrors which was achieved by a Gaussian envelope function [35]. The modulation maximises the Q for the nanobeam by minimising the Fourier components that exist above the light line, i.e. radiation loss into free space. It must be mentioned, another loss mechanism within our system was due to the additional mirror section which tapers into a feeding waveguide. If there are not a sufficient number of airholes in this section, leakage of light from the modulated Bragg mirror section can occur. This leakage was

Optical Materials EXPRESS

minimised by simply adding more airholes within the additional mirror section. Figure 1 shows a cross-sectional view at the cavity centre with a TiO_2 trapezium profile resultant of the etching recipe by Bradley *et al.* [6], and the top-view schematic of the nanobeam showing different sections: additional mirror (A), where the airhole size tapers down and becomes a waveguide; Gaussian mirror (G) and the centre (C).

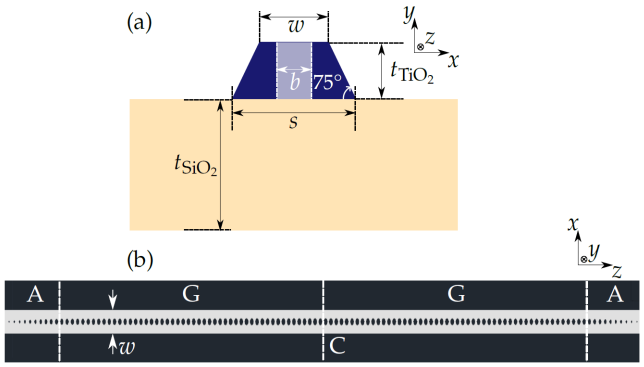

Fig. 1. The geometry of the ultrahigh-Q TiO_2 nanobeam. (a) Cross-sectional trapezium profile which results from Bradley *et al.*'s [6] etching recipe. Here, w and s represent the top and bottom lengths of the TiO_2 trapezium, b is the width of the airhole which changes as you move along the nanobeam in the $\pm z$-direction, t_{TiO_2} and t_{SiO_2} are the thicknesses of TiO_2 and SiO_2 layers. (b) Top-view schematic of the nanobeam with additional mirror (A), Gaussian mirror (G) and the centre (C) shown. Note: the airholes have a tapered profile from the centre of the cavity.

The nanobeam's periodicity consisted of airholes perforating the TiO_2 layer which sits upon an SiO_2 layer. This oxide layer was grown by oxidation of the silicon wafer and we choose to keep this layer as to demonstrate a high-Q cavity is possible in a low refractive index environment. The silicon substrate was not included in the simulations. The resonant wavelength of the nanobeam is chosen to be at the ZPL of the NV^- centre which is 637 nm.

The original design recipe by Quan *et al.* [33, 34] assumed vertical side walls only. Angled side walls was an appropriate consideration since we based the design on the etching recipe in Ref. [6]. The thicknesses of the TiO_2 and SiO_2 were set to $t_{TiO_2} = 0.27$ μm and $t_{SiO_2} = 0.99$ μm. Finally, the refractive indices of TiO_2 and SiO_2 were set to 2.27 and 1.46 respectively.

Three-dimensional FDTD simulations (Lumerical) were performed to determine the Q of the cavity. An electric dipole was placed closed to the centre of the nanobeam cavity at coordinates of $(x, y, z) = (0, 0.2, 0)\mu$m. The spatial grid size was 22 nm; the PML thicknesses were different at each boundary: 2.51 μm (top of nanobeam), 2.37 μm (sides of the nanobeam), and 400 nm (longitudinal directions of the nanobeam). Vertical airholes were considered for all the simulations.

3. Results and discussion

Before exploring the significant enhancement achieved from the nanobeam, it is worth examining the electrodynamics for a simple system first. The emission rate of an emitter in a homogenous refractive index environment can be modified via simple encapsulation in a planar interface environment. The NV^- centre can be approximated as a classical oscillating dipole radiating within a dielectric sphere near an interface [36, 37]. The power radiated by the dipole is inversely proportional to the emitter's fluorescence lifetime. Three-dimensional FDTD simulations (RSoft) were considered for three unstructured environment scenarios: (1) ND in air,

Optical Materials EXPRESS

(2) ND in TiO_2 and (3) ND on TiO_2 in air. The refractive indices were taken to be: $n_{ND} = 2.4$, $n_{air} = 1$ and n_{TiO_2}. The dipole resides at the centre of the spherical ND with a diameter of 60 nm and has an emission wavelength of 637 nm. For scenarios (1) and (2), the dipole is emitting into a homogenous environment. For scenario (3), there is a planar interface between the TiO_2 and the surrounding air. This interface acts as the reference point for parallel (||) and orthogonal ($\perp$) dipole polarisations. The total radiated power by the dipole (P_S) was calculated by summation over the time-averaged Poynting vector of six faces of a cubed power monitor when the simulation had reached a steady state solution. The computational domain size was $1\times1\times1$ μm^3, the spatial grid size was 3 nm and PML was 1 μm for all simulations. The enhancement (ζ) was calculated as the ratio between P_S and the total power radiated from the ND in air (i.e. scenario (1)) for both parallel and orthogonal dipole orientations. Table 1 summarises these numerical FDTD results.

Table 1. The enhancement of parallel and orthogonal dipole polarisations for 637 nm emission in various refractive index distributions. The polarisations are measured with respect to the TiO_2–air interface (scenario 3).

Scenario	$\zeta_{\parallel}$	$\zeta_{\perp}$
ND in air	1	1
ND in TiO_2	18.29	18.27
ND on TiO_2 in air	3.83	1.58

The simulation results show that preferential enhancement in the parallel orientation of the dipole. It shows that if a ND is any high refractive index environment there will be an enhancement of the emission rate without any structured environment such as an optical cavity.

To obtain a sufficiently high-Q cavity, it was found that the Gaussian mirror section should contain fifty airholes (see Figure 1(b), G sections). In addition, to best reflect an experimental situation where the nanobeam can be characterised, an additional mirror (A, see Figure 1(b)) section was also included in the simulations which was tapered down to a feeding waveguide [33]. The additional mirror section consisted of ten airholes. The total length of the nanobeam was then determined to be 20.26 μm, measured from the outer edges of the tenth airholes of the additional mirror sections.

Figure 2 shows the variation in the calculated Q values and their associated resonance wavelengths for vertical sidewalls for the TiO_2 nanobeam cavity. The trend shows that by increasing the number of airholes in the Gaussian mirror, the Q value increases with a blue shifting resonant wavelength. This means that the value chosen for G is arbitrary, any value greater than 40 was sufficient in obtaining a high-Q value. With more airholes this will impart more partial reflections on the light and results in stronger enhancement without sacrificing a large shift in a resonance wavelength. A value of G = 50 was chosen as an appropriate starting point in accomplishing an ultrahigh-Q cavity. The resonance wavelength for G = 50 mirror was found to be 635.15 nm, approximately a 2 nm difference with respect to the ZPL NV^- wavelength. This can be shifted to 637 nm by either: changing the starting or ending filling fractions of the Gaussian mirror (equivalent to changing the radii of the airholes) or adjusting the width of the nanobeam. The latter can drastically shift the resonance wavelength as more modes fall below the substrate light line.

As mentioned in the previous subsection, to best reflect an experimental situation when the TiO_2 is etched, a sidewall angle was considered for the waveguide; this results in the resonance wavelength of the vertical sidewall nanobeam shifting from 635.15 nm. A parameter search of the top and bottom widths of the TiO_2 was conducted to target the 637 nm wavelength with the trapezium profile of the nanobeam. At widths of $w = 0.38$ μm and $s = 0.52$ μm, the L0 TiO_2 nanobeam cavity yielded a $Q = 1.04\times10^7$ with a resonance wavelength of 637.37 nm and

Optical Materials EXPRESS

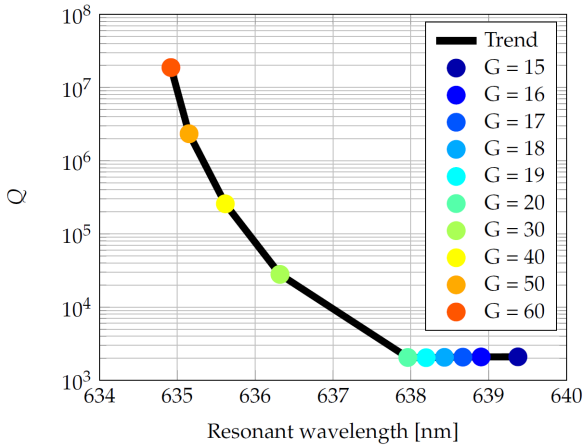

Fig. 2. Q values with their respective resonance wavelengths for the TiO_2 nanobeam as a function of the number of airholes that constitute both Gaussian mirrors (G). The results shown in this figure were for *vertical* sidewalls with a width of $w = 0.44$ μm and a periodicity for the airholes of 0.17 μm.

$V = 3.7(\lambda/n)^3$. This results in a Purcell factor of $F = (3/4\pi^2)(\lambda/n)^3(Q/V) \approx 2.14\times10^5$, a considerably large value.

This represents a substantially large Q for an optical cavity in a low refractive index contrast environment compared to previous work in polymeric nanobeam cavities [38]. However, the modal volume is large due to the presence of the SiO_2 substrate which results low refractive index contrast between ($n_{TiO_2}/n_{SiO_2} = 2.27/1.46 = 1.55$). The refractive index difference between TiO_2 and the SiO_2 substrate is smaller than with TiO_2–air and therefore the mode penetrates into the SiO_2 rather than being reflected back for a high refractive index difference which would be the case for a free-standing nanobeam, i.e. an all air environment.

Figure 3 cross-sectional and top-view power distributions that were calculated for the L0 TiO_2 nanobeam cavity with $w = 0.38$ μm and $s = 0.52$ μm.

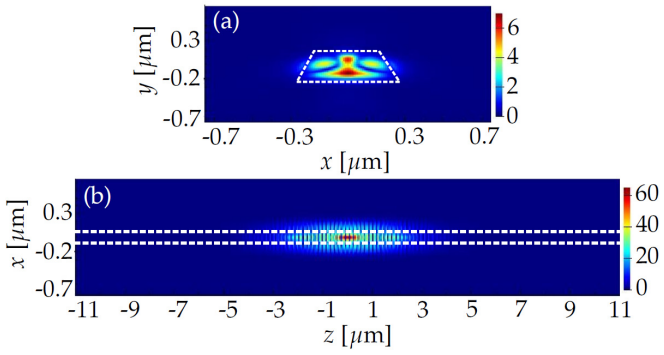

Fig. 3. The power distribution of the TiO_2 nanobeam. (a) Cross-sectional and (b) top-view profiles. The dashed white lines represent the sidewalls of the nanobeam. Note: by default, Lumerical measures the Poynting vector in their power monitors.

The power profiles reveal that the majority within the cavity centre at $(x, z) = (0, 0)$ in Figure 3. The results show that this nanobeam design has the potential to significantly enhance

Optical Materials EXPRESS

the ZPL emission from the NV^- centre for an embedded ND. In the vertical direction (y), the peak power distribution is slightly below the centre of the cavity and therefore this would need to be a consideration when embedding the ND into the growth process of the TiO_2 layer. This is only for the case that an appropriate ND size can be supported between the Gaussian mirrors at the cavity centre.

The results show that an ultrahigh-Q TiO_2 nanobeam cavity can be realised to operate at the ZPL of the NV^- centre for diamond. The Q can be made arbitrarily high by simply increasing the number of airholes that constitute the Gaussian mirrors. This will inherently shift the resonance wavelength slightly, but a parameter search can be conducted on any physical aspect of the nanobeam to re-adjust the resonance wavelength. The only drawback for this short wavelength operation is the critical dimensions of the design become increasingly small which makes it more difficult to fabricate and is limited to current lithographic resolution.

In addition, incidental losses, those not included in the design, will impact the fabricated device. Unintentional refractive index changes can form scattering sites such as grain and mask inhomogeneities. Figure 4 shows a scanning electron micrograph of a the surface of a TiO_2 substrate created via electron-beam deposition that would be considered for the fabrication of the device.

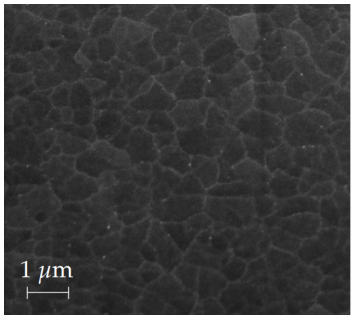

Fig. 4. A scanning electron micrograph of the TiO_2 substrate with embedded NDs.

If a TiO_2 nanobeam was to be fabricated using this particular substrate, the optical loss would be significant, and therefore a reduced Q value, due to scattering of the light because the grain boundaries are significantly smaller compared to the total length of the nanobeam (20.26 μm).

Another point of discussion is the absence of a ND encapsulating the electric dipole, i.e. a ND-TiO_2 interface, within our simulations and incorporating this would be a much more realistic estimation of the physical system. Since the refractive indices of TiO_2 ($n_{TiO_2} = 2.27$) and diamond ($n_{ND} = 2.4$) are comparable, therefore at the interface there will be minimal scattering of the light. McCutcheon *et al.* [39] showed that Q values for silicon nitride ($n = 2.0$) nanobeams reduced by approximately 10–20% from a bare cavity when compared to an embedded 20 nm cubic ND in the cavity centre. In addition, van der Sar *et al.* [40] also explored the positional effects of a ND on the optical properties of gallium phosphide (GaP) S1 and L3 cavities. In this system, the refractive index contrast is much larger because GaP has a refractive index of 3.4. When a ND of 50 nm diameter is placed at the maximum mode intensity of the S1 cavity the original Q value decreases by <10%. When a 60 nm ND is placed at various depths within the GaP substrate, the Q value is greatest near the centre (5% of the original) and decreases near the edges because light is scattered by the ND at the surface is lost from the cavity. Therefore, previous work indicates that ND embedded within a substrate does not significantly change the Q value, only when it's near the surface with a larger refractive index contrast will there be increased losses due to the scattering.

Optical Materials EXPRESS

4. Conclusions

It has been shown that TiO_2 can be a viable material for creating an ultrahigh-Q nanobeam cavity at the ZPL of the NV^- centre. Using the design recipe by Quan *et al.* [33, 34], a Q of 1.04×10^7 at 637.37 nm can be achieved. The Q value can be arbitrarily increased by additional airholes within the Gaussian mirror. This paves the way for TiO_2 to become a future visible photonic material.

Funding

ARC Australian Research Fellowship (DP1096288)

Acknowledgments

K.C. would like to acknowledge an Overseas Research Experience Scholarship provided by The University of Melbourne to visit Prof. Lončar's group. K.C. would also like to thank Jennifer T. Choy, Parag B. Deotare, Qimin Quan, Young-Ik Sohn and Orad Reshef for helpful discussion. The authors would also like to acknowledge Y.H. Leung and A.B. Djurišić for providing the titanium dioxide sample. S.T-H. would like to acknowledge computational resources provided by the Australian Government through NCI under the National Computational Merit Allocation Scheme.